

Replacement of heme by soluble guanylate cyclase (sGC) activators abolishes heme-nitric oxide/oxygen (H-NOX) domain structural plasticity



Aikaterini I. Argyriou^a, Garyfallia I. Makrynitsa^a, Georgios Dalkas^a, Dimitra A. Georgopoulou^a, Konstantinos Salagiannis^b, Vassiliki Vazoura^b, Andreas Papapetropoulos^c, Stavros Topouzis^{b, **}, Georgios A. Spyroulias^{a, *}

^a Department of Pharmacy, University of Patras, GR-26504, Patras, Greece

^b Laboratory of Molecular Pharmacology, Department of Pharmacy, University of Patras, 26504, Patras, Greece

^c Laboratory of Pharmacology, Faculty of Pharmacy, National and Kapodistrian University of Athens, Athens, Greece

ARTICLE INFO

Handling editor: Alexander Wlodawer

Keywords:

Soluble guanylate cyclase (sGC)
Heme
BAY 58-2667
BAY 60-2770
Cinaciguat
H-NOX

ABSTRACT

The gasotransmitter nitric oxide (NO) is a critical endogenous regulator of homeostasis, in major part via the generation of cGMP (cyclic guanosine monophosphate) from GTP (guanosine triphosphate) by NO's main physiological receptor, the soluble guanylate cyclase (sGC). sGC is a heterodimer, composed of an $\alpha 1$ and a $\beta 1$ subunit, of which the latter contains the heme-nitric oxide/oxygen (H-NOX) domain, responsible for NO recognition, binding and signal initiation. The NO/sGC/cGMP axis is dysfunctional in a variety of diseases, including hypertension and heart failure, especially since oxidative stress results in heme oxidation, sGC unresponsiveness to NO and subsequent degradation. As a central player in this axis, sGC is the focus of intense research efforts aiming to develop therapeutic molecules that enhance its activity. A class of drugs named sGC "activators" aim to replace the oxidized heme of the H-NOX domain, thus stabilizing the enzyme and restoring its activity. Although numerous studies outline the pharmacology and binding behavior of these compounds, the static 3D models available so far do not allow a satisfactory understanding of the structural basis of sGC's activation mechanism by these drugs. Herein, application NMR describes different conformational states during the replacement of the heme by a sGC activators. We show that the two sGC activators (BAY 58-2667 and BAY 60-2770) significantly decrease the conformational plasticity of the recombinant H-NOX protein domain of *Nostoc* sp. cyanobacterium, rendering it a lot more rigid compared to the heme-occupied H-NOX. NMR methodology also reveals, for the first time, a surprising bi-directional competition between reduced heme and these compounds, pointing to a highly dynamic regulation of the H-NOX domain. This competitive, bi-directional mode of interaction is also confirmed by monitoring cGMP generation in A7r5 vascular smooth muscle cells by these activators. We show that, surprisingly, heme's redox state impacts differently the bioactivity of these two structurally similar compounds. In all, by NMR-based and functional approaches we contribute unique experimental insight into the dynamic interaction of sGC activators with the H-NOX domain and its dependence on the heme redox status, with the ultimate goal to permit a better design of such therapeutically important molecules.

1. Introduction

Cardiovascular diseases (CVD) are considered the leading cause of death globally according to World Health Organization, with mortality incidence higher than cancer and millions of people hospitalized every year and suffering chronic sequels of CVD. Although several therapies and drugs towards CVD are available, there is urgent need for additional

pharmacological approaches (Gheorghide et al., 2013), resulting in intense research efforts in academia and the pharmaceutical industry (Dasgupta, Bowman, D'Arsigny and Archer, 2015). Oxidative stress is identified as a crucial causal factor in several CVDs and has been well-described to disrupt vasculoprotective networks, including the nitric oxide/cyclic guanosine monophosphate (NO/cGMP) signaling pathway (Stasch et al., 2006).

* Corresponding author.

** Corresponding author.

E-mail addresses: stto@upatras.gr (S. Topouzis), G.A.Spyroulias@upatras.gr (G.A. Spyroulias).

<https://doi.org/10.1016/j.crstbi.2021.11.003>

Received 17 September 2021; Received in revised form 3 November 2021; Accepted 5 November 2021

2665-928X/© 2021 The Author(s). Published by Elsevier B.V. This is an open access article under the CC BY-NC-ND license (<http://creativecommons.org/licenses/by-nc-nd/4.0/>).

NO is an endogenously generated diatomic molecule, whose best-described signaling activity involves the activation of the enzyme soluble guanylate cyclase (sGC), which converts GTP to cGMP to thus effect downstream changes in cellular homeostasis (Dang et al., 2020). sGC is a heterodimer enzyme composed of two subunits, α and β , each consisting of 4 distinct domains: the N-terminal “receptor” domain, followed by a Per/Arnt/Sim (PAS) domain, a coiled-coil domain and a catalytic domain. The N-terminal domain of the regulatory $\beta 1$ subunit is a Heme-Nitric oxide/Oxygen sensing (H-NOX) domain associating with one heme molecule and displaying high sensitivity towards NO, while the corresponding domain of the $\alpha 1$ subunit is a “pseudo” H-NOX domain with no such ability and ambiguous function (Ma et al., 2007). NO binds upon the Fe^{2+} -carrying heme of $\beta 1$ H-NOX domain, resulting in a series of conformational and charge changes which lead to the enzymatic activation of sGC. Loss of the heme co-factor (e.g. by oxidation of the Fe^{2+}) or reduced bioavailability of its main ligand, NO, results in a dysfunctional and/or NO-unresponsive sGC enzyme and consequently in an impaired NO/cGMP pathway.

Besides the classic NO donor drugs such as glyceryl trinitrate, intense research has succeeded in designing and synthesizing novel classes of sGC modulators with therapeutic properties. So far, two differently-acting classes of such compounds have been proposed to restore the activity of dysfunctional sGC: heme- and NO-dependent sGC “stimulators” and heme- and NO-independent sGC “activators”. Although stimulators can trigger the cGMP production in a NO-independent manner through the binding on the heme-containing enzyme, their activity seems to be greatly enhanced in the presence of endogenous NO, even at low levels, leading to important synergy. On the contrary, sGC activators act on a heme-free or heme-oxidized sGC, rendering the enzyme functional again and stemming its degradation by the proteasome, for example under conditions of oxidative stress (Breitenstein et al., 2016). The approval of compounds such as the sGC stimulator Riociguat (trade name: Adempas) (Mittendorf et al., 2009; Ghofrani et al., 2013) provides clinical proof of the clinical utility of these classes. In contrast, sGC “activators” have thus far failed to reach clinical approval, e.g. Cinaciguat or Ataciguat (Schindler et al., 2006 and reviewed in Sandner et al., 2021). The exact mechanism employed by sGC activators is still largely elusive and constitutes the focus of intense research efforts. As far as their binding site within the H-NOX domain is concerned, the available 3D structures of H-NOX domain in complex with activators (PDB id: 3L6J, 4JQH, 4IAE) (Martin et al., 2010; Kumar et al., 2013) provide evidence that these molecules replace heme in the core of the protein structure and offer valuable information on the residues interacting with the compounds. That said, little is known about the conformational rearrangements and the sequential dynamic events taking place during the binding with the activators.

In the present study, we demonstrate for the very first time the dynamic nature of the H-NOX domain in its native complex form (i.e. with heme) and during the binding of two sGC activators (BAY 58-2667 and BAY 60-2770) with similar organic skeleton, using as a model the H-NOX domain from *Nostoc* sp. cyanobacterium (*Ns* H-NOX). Specifically, we shed light on the dynamic properties of the H-NOX domain in different time-scales, both in the heme-bound state and in the presence of the activators, by integrating NMR approaches and molecular dynamics methodologies. We also provide functional evidence based on NMR and cellular cGMP generation that even similar molecules can diverge mechanistically in their interaction with the H-NOX domain and with the sGC holoenzyme and that this interaction is reversible, bi-directional and competitive with reduced heme. The present data will help optimize the design of sGC agonists and contribute a better insight into their utility in relevant pathophysiological states.

2. Methods

2.1. Protein sample preparation

The experimental protocol for the expression, purification and NMR sample preparation of the *Ns* H-NOX C139A variant (residues M1-D183) has been reported previously (Alexandropoulos et al., 2016). Heme replacement by BAY 58-2667 and BAY 60-2770 has been described elsewhere (Martin et al., 2010). Protein concentration of the ^{15}N -labeled protein in the samples for the titration experiments was 0.6 mM, for the CEST experiments and for R_2 measurements during the titration with BAY 58-2667 was 1 mM. For the titration experiments in the presence of the antioxidative agent, 5 mM of L-ascorbate was added right before the chemical compounds.

2.2. NMR spectroscopy

All NMR experiments acquired on a Bruker Avance III HD four channel 700 MHz NMR spectrometer at 298 K, equipped with TCI 5 mm $^1\text{H}/^{13}\text{C}/^{15}\text{N}/\text{D}$ -gradient probe. All data sets were processed with Topspin 3.5 software and analyzed with CARRA (Keller, 2004). Backbone and side chain assignment of the heme-bound (Alexandropoulos et al., 2016) and BAY 58-2667 (Makrynitsa et al., 2021) *Ns* H-NOX protein have reported in previous studies.

2.3. NMR titration experiments

To monitor the behavior of the individual amino acids of the ^{15}N -labeled *Ns* H-NOX in the presence of BAY 58-2667 or BAY 60-2770, we calculated the changes of their chemical shifts in $^1\text{H}-^{15}\text{N}$ HSQC spectra during the NMR titration experiment. The unlabeled ligand (compound stock concentration=50 mM) was added in 4 steps in order to reach excess of each BAY in the protein sample. Chemical shift perturbation (CSP) values were calculated using the equation $\Delta\delta_{ppm} = \sqrt{(\Delta\delta_{HN})^2 + (\frac{\Delta\delta_N}{5})^2}$. The threshold was defined by calculated the standard deviation σ , exclude any residue with CSP greater than 3σ and then recalculate σ (Williamson, 2013).

2.4. Protein dynamics

The backbone dynamics of the heme-bound H-NOX protein and on the H-NOX complexes with each of the activator compounds were studied on the ps-ns time scale through the analysis of ^{15}N R_1 and R_2 relaxation rates and hetero-nuclear $^1\text{H}-^{15}\text{N}$ NOES. A series of 2D spectra in a pseudo-3D mode were recorded with relaxation delays of 20 ms, 60 ms, 100 ms, 200 ms, 400 ms, 600 ms, 800 ms and 1200 ms for R_1 relaxation rate. Relaxation delays for the R_2 were 15.68 ms, 31.36 ms, 62.72 ms, 94.08 ms, 125.44 ms, 156.8 ms, 188.16 ms and 219.52 ms. All the relaxation data were analyzed with Bruker's Dynamic Center software.

2.5. CEST experiment and data fitting

^{15}N -CEST experiments (Vallurupalli et al., 2012) were acquired as a series of 2D spectra in a pseudo-3D mode and recorded with a mixing time 400 ms and a B1 radiofrequency field of 14Hz applied at the ^{15}N dimension in steps of 28Hz. CEST data were analyzed using the Bruker's software, Dynamic Center.

2.6. Molecular dynamics

The crystal structure coordinates of the *Ns* H-NOX were obtained from

the PDB with accession code: 4IAM. The Metal Center Parameter Builder (MCPB) program (Li and Merz, 2016) has been used to build force fields for the simulation of *Ns* H-NOX/heme complex. Force-field parameters for the ligands BAY 58-2667 and BAY 60-2770 were prepared using the ANTECHAMBER package (Susa da Silva & Vranken, 2012) and the AM1-BCC atomic charges (Jakalian, Jack & Bayly, 2002). The ff14SB (Maier et al., 2015) force-field parameters and the General-Amber Force-Field (Wang et al., 2004) were applied to the structure atoms. MD simulations were performed using the GPU-accelerated version of PMEMD in AMBER18 (Case et al., 2018). The Particle Mesh Ewald method (Darden, York & Pedersen, 1993) was used for long-range electrostatic interactions with a real space cut-off of 9 Å.

A three-stage equilibration protocol, consisting of energy minimization and MD simulations, was used to eliminate any unfavourable interactions and to gently adjust the starting complex to the molecular mechanics force field prior to production of MD simulations. The calculations for all the systems were carried out using the same simulation parameters.

The SHAKE algorithm (Ryckaert, Ciccotti & Berendsen, 1977) was used to constrain bonds involving hydrogen with a relative tolerance of 1×10^{-7} . CPPTRAJ (Roe and Cheatham, 2013) as used to find and track hydrogen bonds over the course of the trajectories, using for both distance and angle cut-offs the default values for hydrogen bonds of the CPPTRAJ module. VMD 1.9.2 (Humphrey, Dalke & Schulten, 1996) was used to visualize the trajectories and prepare the figures.

MD-derived N–H order parameters (S^2) were calculated using the isotropic reorientational eigenmode dynamic analysis (iRED) (Prompers and Brüschweiler, 2002). The covariance matrix of the N–H bond vectors was obtained from the trajectories using the CPPTRAJ module. A total of 50,000 snapshots for each complex with a 20 ps sampling frequency were used for order parameters estimates. The order parameters were calculated as averages over a sliding window of 10 ns. The 10 ns time window was selected because the length of the simulation time exceeds the overall tumbling correlation time of the protein, which is 9.5 ns and MD-derived order parameters calculated over the whole simulation time can include motions that would not be reflected in the experimental NMR order parameters, leading to a bias in the computed S^2 values.

2.7. Cell-based cGMP determination

A7r5 rat aortic smooth muscle cells (RAoSM) and LnCaP human prostate cancer epithelial cells (both from ATCC, Rockville, MD) were cultured in 48-well clusters in DMEM and RPMI growth media (Gibco™), respectively, supplemented with 10% Fetal Bovine Serum (Gibco™) and 1% Penicillin/Streptomycin. (Biosera).

After reaching confluence, cells were serum-starved for 2 h in serum-free media containing 0.1% BSA, whereupon they were pretreated with the heme-oxidizing compound 1H-[1,2,4]oxadiazolo[4,3-a]quinoxalin-1-one (ODQ) (Cayman Chemicals) at 10 μM or its vehicle control (DMSO) for 20 min. After a washout with serum-free media, cells were exposed to the non-selective phosphodiesterase (PDE) inhibitor isobutylmethyl-xanthine (IBMX, 1 mM) (Applichem) for 5 min. They were then exposed to the sGC activators BAY 58-2667 or BAY 60-2770 (10 μM) (both a generous gift of BAYER) or the heme-dependent NO donor SNP (Applichem), for 15 min.

In the experiments where the influence of L-ascorbate (Applichem) was assessed, after the incubation with IBMX, cells were exposed to the activator BAY molecule, with L-ascorbate or vehicle Control (medium) being added either simultaneously or at the indicated times after BAY addition, until cell extract collection.

The extracts were collected by HCl 0.1M and analyzed by a commercial ELISA kit (Cayman Chemicals) for total cell cGMP content, following the manufacturer's instructions. cGMP levels were normalized for total protein in the respective well, determined by a Micro BCA Protein assay kit (Thermo Scientific).

3. Results

3.1. Solution NMR study of the heme replacement by BAY 58-2667 and BAY 60-2770

For the NMR experimentation, we used as a model the recombinant H-NOX domain from the bacterium *Nostoc* sp. The 3-D structure of the sGC β-subunit H-NOX domain is remarkably well-conserved among species, while the amino acids of the H-NOX cavity which mediate the interaction of H-NOX with heme are remarkably well-conserved between bacterial and mammalian species (e.g. *Nostoc punctiforme*, *Bos taurus*), being identical by ~63% (17 of 27, (Alexandropoulos et al., 2016; Makrynitsa et al., 2019; Wittenborn and Marletta, 2021)). This is why rational drug design based on microbial H-NOX structural data and on the very structure of heme has contributed to, and still informs, the development of sGC activator molecules all the way to advanced clinical trials (reviewed in Alexandropoulos et al., 2016; Makrynitsa et al., 2019; Liu et al., 2021; Wittenborn and Marletta, 2021)). Despite all this, it is understood that ideally, any conclusions derived from a structural approach using a recombinant microbial domain (in this case *Nostoc* sp. H-NOX) should seek additional corroboration by functional studies probing the activation of the sGC holoenzyme.

Initially, we investigated the binding behavior of these chemical compounds through NMR-driven titration experiments. According to the analysis, after BAY 58-2667 addition, 58 residues exhibited CSP above the threshold. In comparison, 56 residues showed similar perturbations when BAY 60-2770 was used (Fig. 1A–D). Mapping of the affected residues on the 3D structure of *Ns* H-NOX domain (PDB ID: 4IAM) (Kumar et al., 2013) shows that the amino acids affected are almost identical in both cases and that most of them are located around the heme cavity, indicating a specific binding mode for both compounds (Fig. 1E and F), which seem to occupy the interior core of the protein. It is worth noting that the changes on the backbone NH chemical shift values are a direct consequence of the replacement of the heme by the compounds, resulting in the formation of a new biomolecular complex.

In a previous study (Makrynitsa et al., 2021), we described the difference on the assignment percentage (backbone and side chain) of the heme-bound H-NOX and H-NOX in complex with BAY 58-2667, in relation with the quality of the acquired NMR data. The quality of the acquired data for the H-NOX-BAY complexes is distinctly superior to the native heme-loaded H-NOX in terms of peak population, intensity and peaks half-width. The H-NOX-BAY complexes yielded well-resolved spectra with narrow, intense peaks which allowed a considerably higher degree of resonance identification, compared to the native H-NOX. These observations are also strongly coupled with the ^{15}N -relaxation properties of the protein which is discussed further in the text and concern residues mainly, but not exclusively, around the heme moiety. Regions W74-Y77 and L101-V108, forming the two α-helices above and below the heme, respectively, were unassigned in the heme-bound H-NOX protein, but their resonances were easily identified in the BAY 58-2667 complex. Also, it is worth mentioning that there are certain residues around the heme cavity adopting a second conformation according to the analysis of the ^1H - ^{15}N HSQC (Fig. 3D–G).

3.2. Heme replacement by activators affects the dynamic properties of the H-NOX protein domain

To complement the information on conformational fluctuations obtained via NMR order parameters for the H-NOX backbone, we carried out a series of MD simulations that probe the intramolecular dynamics (Prompers and Brüschweiler, 2002) of all parts of the heme-bound *Ns* H-NOX and BAY activator-bound *Ns* H-NOX and obtained a total of 1 μs of simulation data for all three complexes. There is remarkable, but not total, residue-by-residue agreement between the backbone S^2 values determined by NMR and MD for each complex (Suppl. data Fig. 1A–C). Backbone order parameters are reproduced with similar accuracy for the

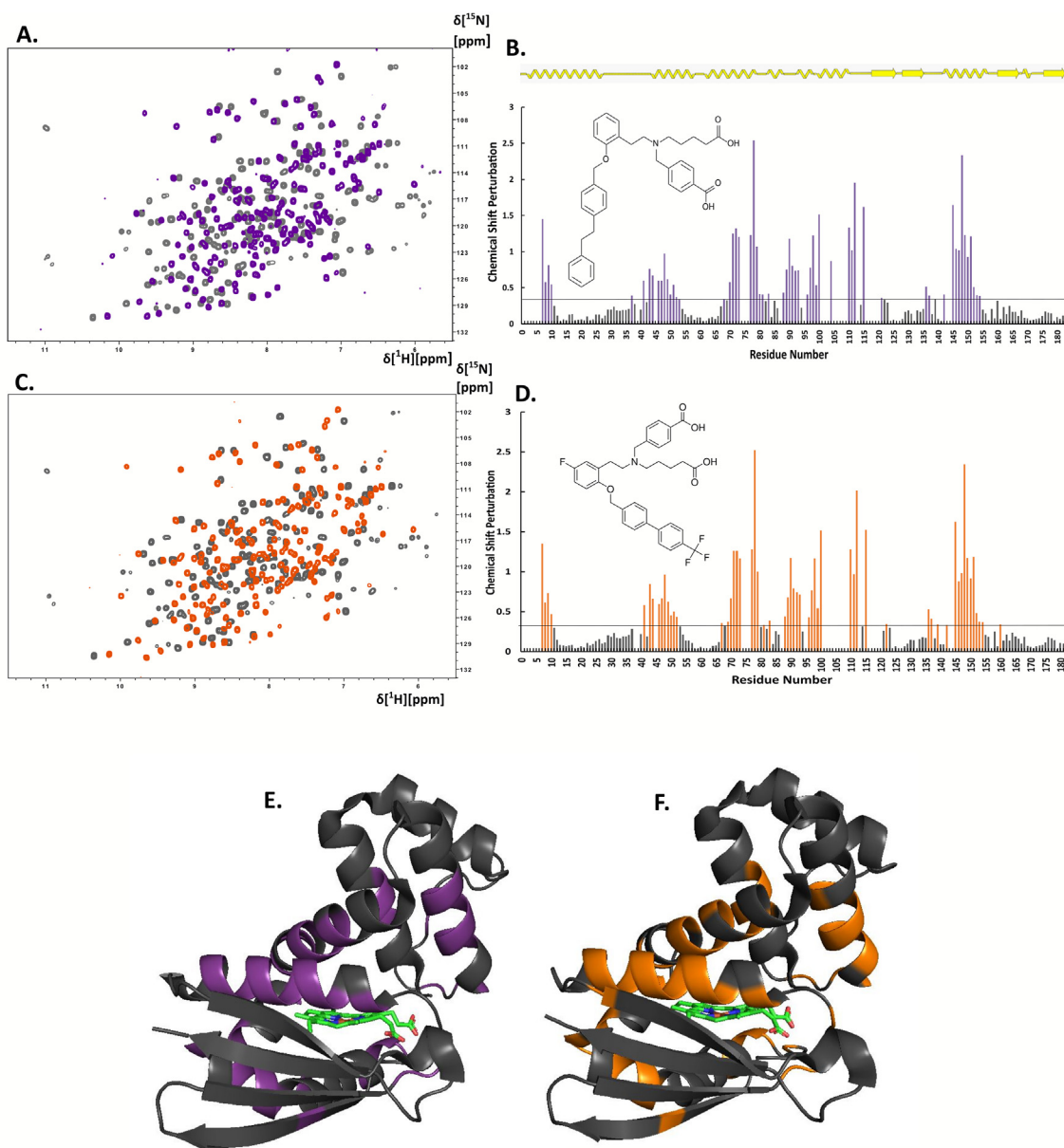


Fig. 1. A. Overlay of ^1H - ^{15}N HSQC spectra of the Ns H-NOX domain in heme-bound state (grey) and BAY 58-2667 bound state (purple). B. Top panel: Secondary structure of X-ray structure Ns H-NOX. CSP in response to BAY 58-2667 binding with threshold value 0.33. C. Overlay of ^1H - ^{15}N HSQC spectra of the Ns H-NOX domain in heme-bound state (grey) and BAY 60-2770 bound state (orange). D. CSP in response to BAY 60-2770 binding with threshold value 0.32. E., F. Ribbon representation of the X-ray structure of Ns H-NOX domain (PDB id: 4IAM). The residues with CSPs above the threshold are mapped onto the surface using the same color code as in A and B. (Ribbon representations were generated by UCSF Chimera software) (Pettersen et al., 2004). (For interpretation of the references to color in this figure legend, the reader is referred to the Web version of this article.)

native, heme-bound and Ns H-NOX/BAY 58-2667 and Ns H-NOX/BAY 60-2770 states with an RMSD of 0.1, 0.09, 0.08 respectively, indicating a good overall agreement. The mean value of the backbone order parameters is 0.86 ± 0.02 for all three complexes. The dynamical characterization using MD methods indicated distinct differences in Ns H-NOX's flexibility upon ligand binding. On the μs time-scale, all complexes showed high flexibility in loops L1 and L4, while significantly enhanced dynamics were observed for residues in loops L2 and L3 and helix αF (Suppl. data Fig. 1D and E). Interestingly, several of these residues display chemical shift changes upon heme replacement by BAY 58-2667 or BAY 60-2770 and formation of these new complexes; however, many residues that show shift changes do not exhibit changes in S^2 . It should be noted that residues around the sequential stretches of unassigned residues of Ns H-NOX/heme have low values of S^2 , suggesting that these

regions undergo an exchange between two different conformational states on an intermediate μs -ms time scale. Hydrogen bond analysis was also employed to examine the stability of the BAY compound-complexed H-NOX at the ms timescale. Examination of the MD trajectories of the two complexes revealed that the carboxyl-butyl moiety of the BAYs participates in extensive and remarkably stable hydrogen bonds and salt-bridge interactions with the conserved YxSxR motif of H-NOX domain. An additional strong hydrogen bond that was observed for over 80% of the simulation time was also formed between the ether oxygen moiety of BAYs and the NH proton of the W74 pyrrole moiety. Furthermore, the hydrophobic moieties of both BAYs make extensive and stable hydrophobic interactions with many hydrophobic residues within the heme-binding pocket, including during the course of the simulation time, enhancing the stability of the insertion of the compounds in the active

site of the protein (Suppl. data Fig. 1F and G) (Kumar et al., 2013). While the MD simulations do not precisely reproduce the NMR order parameters for individual residues, they are clearly capable of capturing the trends along the protein sequence with very good agreement with NMR, indicating in a preliminary way the importance of the dynamic properties of this protein.

To gain more detailed insights into the dynamic properties of the H-NOX protein and determine whether the differences on the assignment percentage between the native (H-NOX-heme) and the BAY-H-NOX complexes is indeed due to variability in conformational flexibility, we performed NMR dynamics experiments on the three complexes. Analysis

of ^{15}N NMR relaxation data, shows that heme-bound *Ns* H-NOX domain in solution and in complex with BAY 58-2667 or BAY 60-2770 exhibits a rather rigid structure in the ps-ns time scale (Suppl. data Figs. 2 and 3). The average HeteroNOE values of the heme-bound H-NOX domain and the BAY 58-2667- and BAY 60-2770-H-NOX complexes are 0.77 (calculated for the 148 assigned residues), 0.86 (calculated for the 169 assigned residues) and 0.89 (calculated for the 168 assigned residues), respectively. Significant differences are detected mainly around the heme cavity, with the regions A63-E81, S93-F112 and L141-Q157, comprising three α helices surrounding heme, exhibiting lower average HeteroNOE values in the native H-NOX complex compared to the respective values

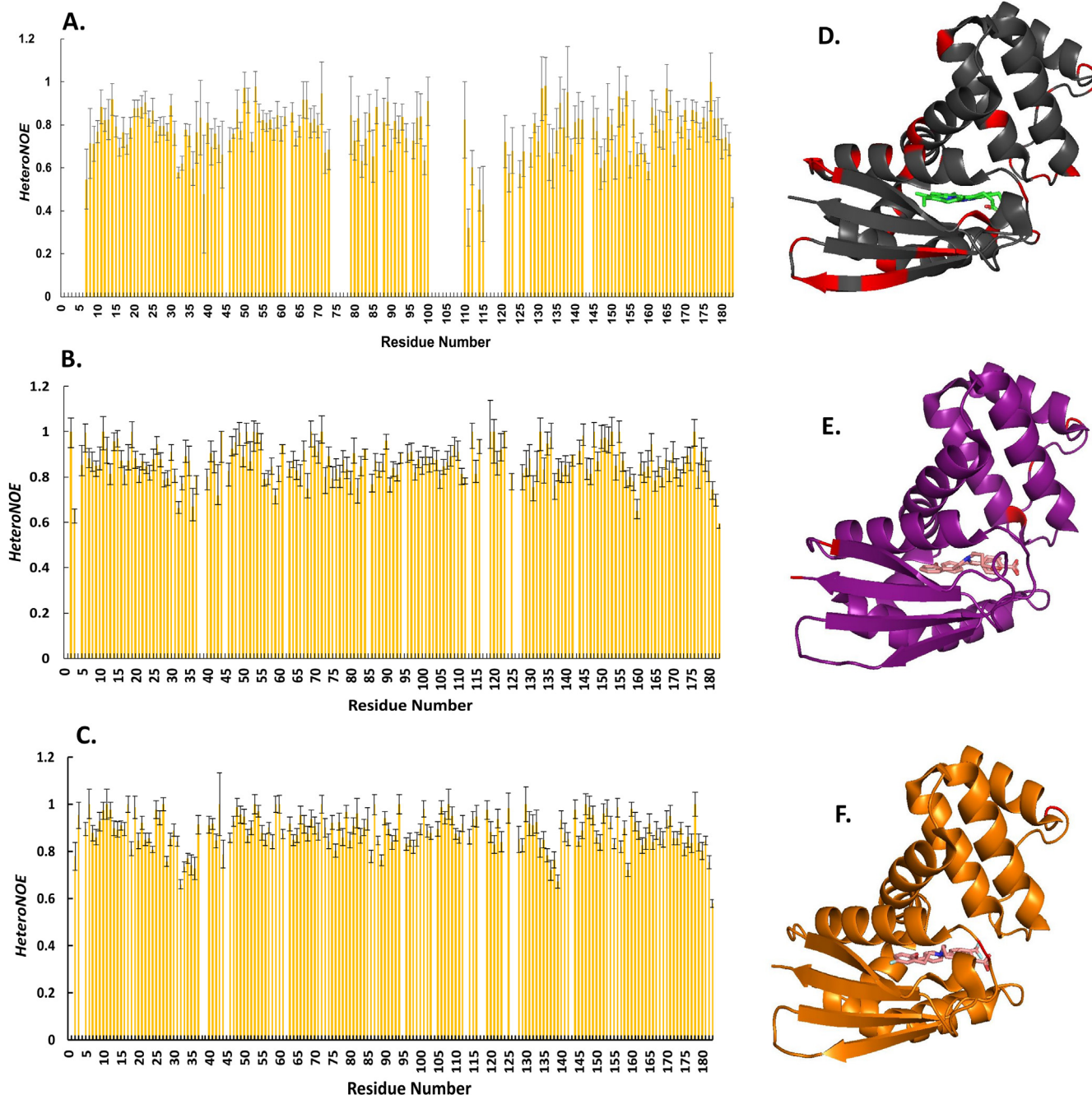


Fig. 2. Backbone *HeteroNOE* values, determined by NMR relaxation experiments for **A.** *Ns* H-NOX/heme, **B.** *Ns* H-NOX/BAY 58-2667, **C.** *Ns* H-NOX/BAY 60-2770. Ribbon representation of the X-ray structure of **D.** *Ns* H-NOX domain (PDB id: 4IAM), **E.** in complex with BAY 58-2667 (PDB id: 3L6J), **F.** in complex with BAY 60-2770 with the residues with *HeteroNOE* values lower than 0.7 colored with red. (For interpretation of the references to color in this figure legend, the reader is referred to the Web version of this article.)

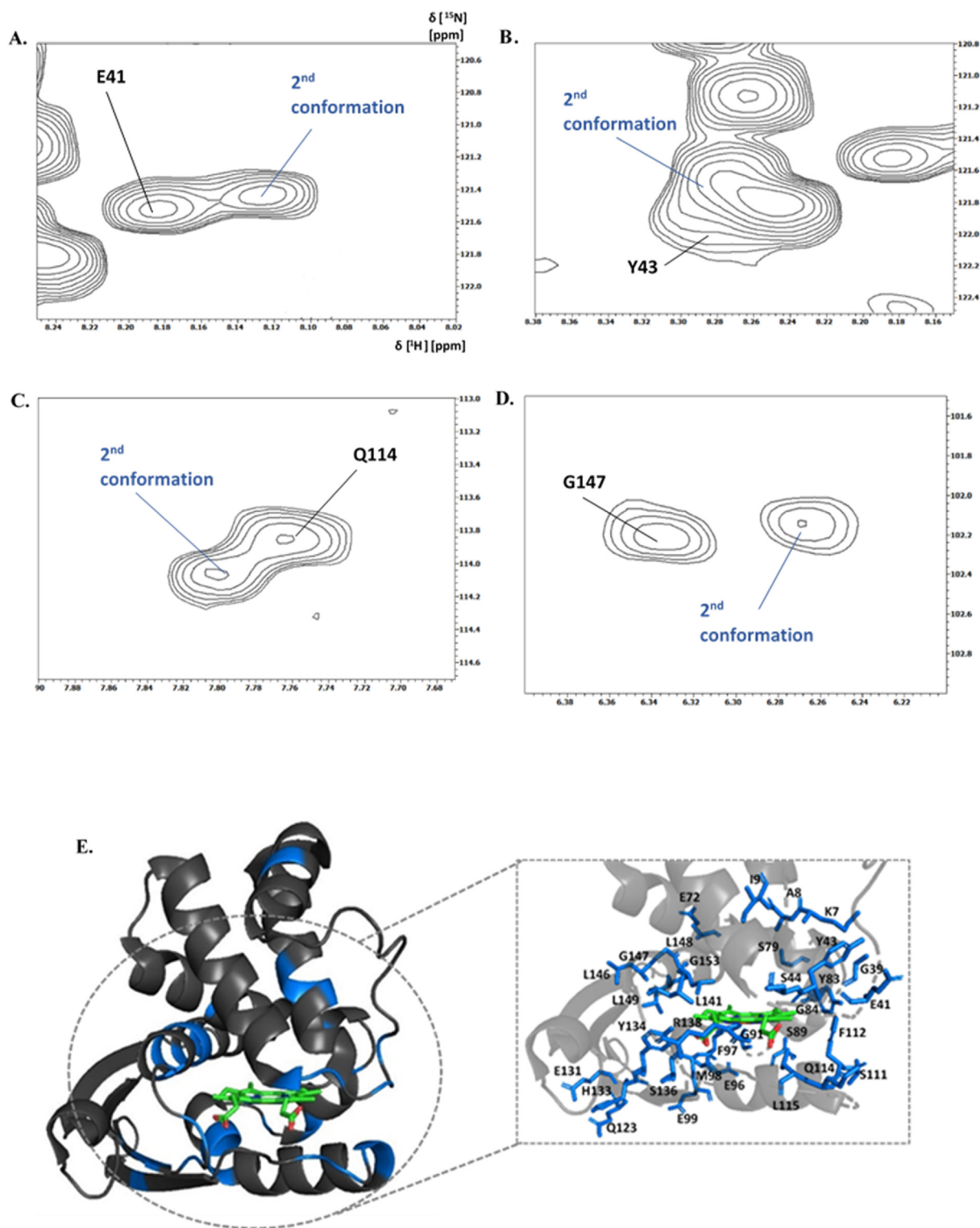


Fig. 3. A-D. ^1H - ^{15}N HSQC regions indicating the second conformation of E41, Y43, Q114, G147. E. Ribbon representation of X-ray structure of the heme bound Ns H-NOX. Residues with second conformation in HSQC are colored with blue. (For interpretation of the references to color in this figure legend, the reader is referred to the Web version of this article.)

obtained with the two others complexes. (Fig. 2, Table 1). The correlation times τ_c for the three complexes are: 9ns (Ns H-NOX/heme), 10.1ns (Ns H-NOX/BAY 58-2667) and 9.2ns (Ns H-NOX/BAY 60-2770), indicating that the protein (molecular weight: 20 kDa) behaves as a spherical protein in all the states.

3.3. NMR reveals different conformational states of the H-NOX protein domain

By comparing the average values, it is obvious that the heme has a significant impact on the protein flexibility concerning the residues

Table 1

Average HeteroNOE values for the three helices close to heme pocket in heme, BAY 58-2667 and BAY 60-2770 bound states.

	helix A63- E81	helix S93- F112	helix L141- Q157
heme-bound H-NOX	0.80	0.72	0.77
BAY 58-2267-bound H-NOX	0.86	0.86	0.90
BAY 60-2770-bound H-NOX	0.90	0.87	0.90

forming the heme cavity. Furthermore, insertion of either compound results in a more rigid and stable H-NOX protein. Moreover, in the case of the heme-H-NOX complex, residues around the sequential stretches of unassigned residues have low *HeteroNOE* (Fig. 2A–C) and S^2 values (Suppl. data Fig. 1A–C) suggesting that these regions undergo an exchange between two different conformational states on an intermediate, μ s–ms, scale. Finally, a close-up view of the ^1H - ^{15}N HSQC spectrum of the protein in the native state reveals that several residues around the heme exhibit two conformational states, while in complexes with the BAY compounds this effect is totally absent (Fig. 3A–D, Suppl. data Fig. 4).

The observable line broadening is due to millisecond time-scale conformational transitions, indicating the presence of alternate conformational states (Alderson and Kay, 2020). For a quantitative understanding of the exchange process, we applied chemical exchange saturation transfer (CEST) spectroscopy. It is noteworthy that the ^{15}N -CEST approach could identify 20 residues of the heme-H-NOX with minor dip in their CEST profile, which share the same surface around the heme moiety with the residues that undergo second conformation in the ^{15}N -HSQC spectrum or they are close to the unassigned regions (Fig. 4A–E). We conducted the same experiment on the *Ns* H-NOX/BAY 58-2667 complex to identify the effect of the exchange. Only 4 of the previously identified residues (Y43, T48, L86, S136) are also undergoing exchange in this complex as well, however we could identify 14 additional residues that exhibit the exchange effect. In both complexes (heme-H-NOX and BAY 58-2667/H-NOX), residues undergoing this exchange are located mainly around or close to the heme-binding (or BAY 58-2667-binding) cavity, stressing the high conformational exchange mode of this area, which may be responsible for determining the bioactivity outcome (Fig. 4A–D, F). In the case of the heme-H-NOX complex, residues indicated in Fig. 4A–D displays low HeteroNOE values and share common dynamic properties, adopting a second visible conformation in the ^1H - ^{15}N HSQC spectrum and an “invisible” state (suggested by the CEST).

Due to the sensitivity of R_2 to slow conformational exchange (Eisenmesser et al., 2002), we performed direct measurements of R_2 during the titration with BAY 58-2667. It became evident that 15 backbone amide nitrogens out of 148 exhibit an increase in R_2 (Fig. 5A), thus identifying regions on the protein that undergo micro-to millisecond dynamics due to the heme replacement by BAY 58-2667 and the formation of a new, more stable complex. Three residues (F36, L110, V145) display the most significant increase of R_2 value (Fig. 5B–D) during the titration with BAY 58-2667. All of them are close either to residues with high CSP values or residues displaying a prominent CEST effect, reinforcing the view that initially protein regions around the heme adopt a very flexible mode with highly conformational exchange behavior. This enables an appropriately accommodating conformation during the replacement of the heme by BAY 58-2667, which permits oxidized heme to leave the protein, while subsequently allowing the chemical activator to take its place in the heme cavity.

3.4. L-ascorbate affects heme replacement by the BAY sGC activators

Based on the extensive structural analysis described above, we hypothesized that there is a dynamic exchange/competition between the heme moiety and the sGC “activator” molecules for occupation of the same H-NOX protein cavity space. In addition, we wanted to test whether

this exchange is bi-directional, i.e. whether the replacement of the oxidized heme moiety in the cavity by the activator molecule is reversible if the oxidation of the heme is stopped or inversed by an anti-oxidant.

Thus, we performed NMR-driven titration experiments to monitor the effect of L-ascorbate on replacement of the heme by BAY 58-2667 and BAY 60-2770. In initial studies, we confirmed that there is no direct modification of either activator by L-ascorbate (results not shown), and thus any effect observed can be logically attributed to L-ascorbate prevention of heme oxidation in our system. The antioxidant agent had a significant impact on the ability of both activators to occupy the heme cavity of H-NOX. Please note that the spectra of the activators in complex with H-NOX in the absence of L-ascorbate are presented in a previous Figure (Fig. 1A and C) and therefore one needs to compare spectrum in Fig. 6A with that in 1A and spectrum 6D with the one depicted in 1C. As can be seen in Fig. 6B, while BAY 58-2667 is able to replace heme really fast in the absence of L-ascorbate, in its presence (Fig. 6A) it is unable to fully integrate the complex and even at the highest concentration used (3.5 μ moles BAY 58-2667), the percentage replacement is far from complete (being only 50%, Fig. 6C). BAY 60-2770's ability is also affected by L-ascorbate. In higher concentrations of BAY 60-2770 in the presence of L-ascorbate, most of the peaks are missing in the NMR spectrum, implying that there is no stable complex with activator and the protein loses its folding (Fig. 6E and F). The data, in all, show that when L-ascorbate is added, the complexes of H-NOX with the activators are not easily detected by NMR, denoting a “collapse” of the complexes and an inability to maintain an NMR-compatible (more stable) conformation. For this reason, based solely on these data, we cannot directly compare the respective degree of complexation of BAY 58-2667 and BAY 60-2770 with H-NOX when L-ascorbate is present, since the methodology does not allow “visualisation” of relevant amino acids in this more “fluid” complex. This interference of L-ascorbate with the ability of the activators to form a complex with H-NOX is further supported by analyzing other amino acids as well, that reflect the degree of complexation of each activator with the H-NOX protein (Suppl. data Fig. 5).

3.5. Effect of L-ascorbate on cGMP generation by the BAY activators *in vitro*

To address whether the remarkable effect of L-ascorbate on the formation of the H-NOX complexes that we observed has functional consequences on the activity of the sGC holoenzyme, we studied also the activity of these compounds in the presence of L-ascorbate in a cell-based cGMP generation enzymatic assay. For this reason, we initially examined if the ability of BAY 58-2667 and BAY 60-2770 to increase cGMP levels is indeed enhanced by the loss of the heme from the sGC protein, to confirm their reported profile as “heme-independent sGC activators” (Kumar et al., 2013; Sömmer et al., 2018; Ghosh et al., 2014; Kollau et al., 2018). We chose to use the A7r5 smooth muscle cell line, which has been previously reported to respond well to sGC agonists (Holt et al., 2016). The dissociation and loss of the heme moiety was triggered by its oxidation following treatment with 1H-[1,2,4]oxadiazolo[4,3-a]quinoxalin-1-one (ODQ), as described previously (Chester et al., 2011; Hoffmann et al., 2009). Cellular cGMP levels served as the biological end-point of sGC activation. In the assay, we included the NO donor sodium nitroprusside (SNP), whose activity, in contrast to the sGC “activators”, is known to be heme-dependent (Zhou et al., 2008). Of note, ODQ by itself did not significantly affect basal cGMP levels.

Indeed, the raise of cGMP levels by SNP was nearly abolished in cells pretreated with ODQ (Suppl. data Fig. 6A). In contrast, pretreatment with ODQ and loss of the heme resulted in significant, several-fold potentiation of the activity of the sGC agonists BAY 58-2667 and BAY 60-2770 (Suppl. data Fig. 6A), confirming their mode of action as sGC “activators” (Follmann et al., 2013; Evgenov et al., 2006; Papapetropoulos et al., 2015). It is worth noting that BAY 60-2770 is more effective than BAY 58-2667 at equal concentration, whether the cGMP-raising effects of the two molecules are compared in “naïve” (ODQ-untreated) cells or

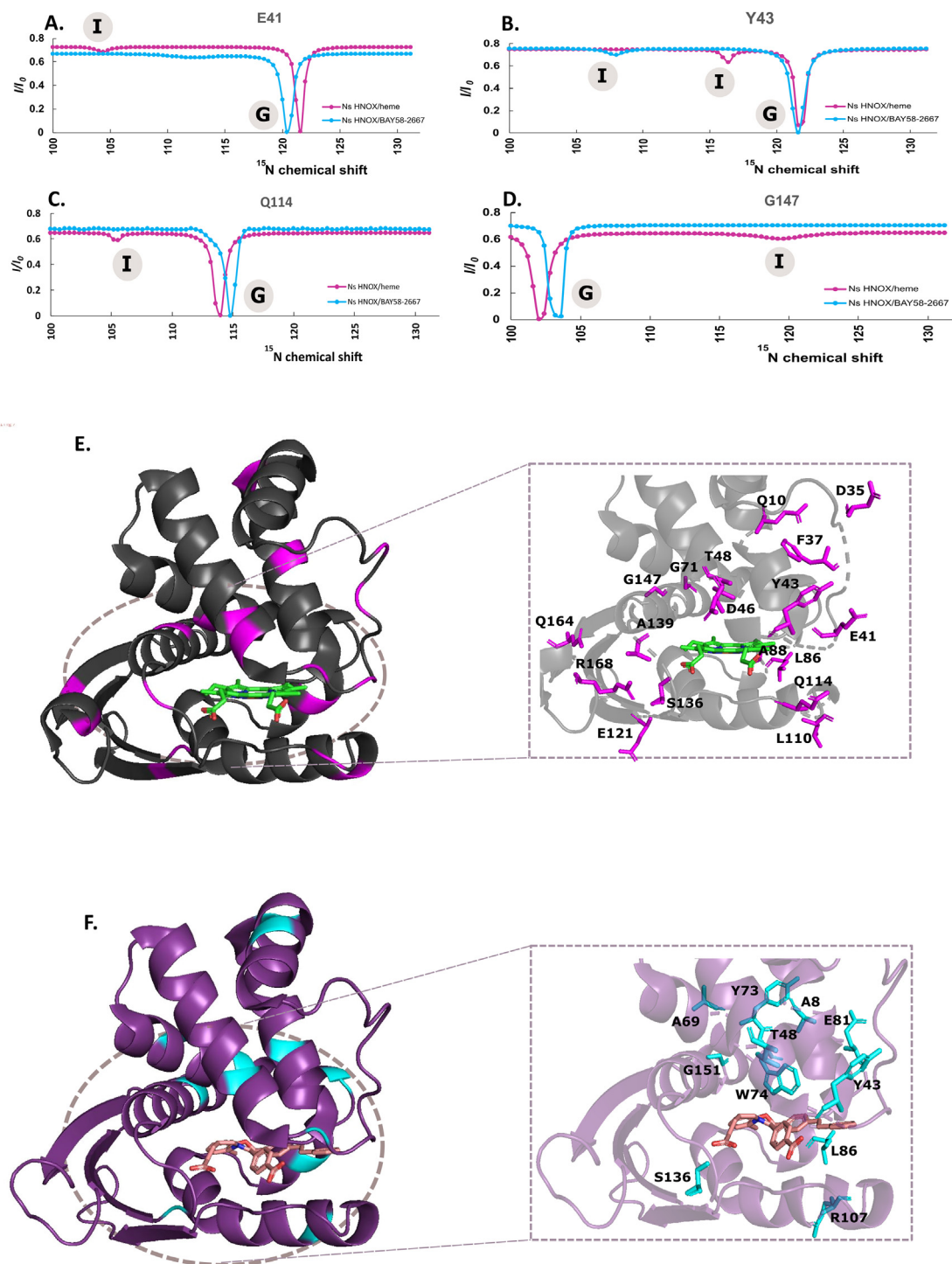


Fig. 4. A-D. ^{15}N -CEST profiles of residues E41, Y43, Q114, G147 of *Ns* H-NOX domain in heme-bound state (magenta) and in complex with BAY 58-2667 (cyan) (I: invisible state, G: ground state). Population of the invisible for the residues are E41 $p=3\%$, Y43: $p=2.5\%$ (heme bound), $p=1\%$ (BAY 58-2667), Q114: $p=3.5\%$, G147: $p=2\%$. E. Ribbon representation of X-ray structure of the heme bound *Ns* H-NOX. Residues with CEST are colored with magenta. F. Ribbon representation of X-ray structure of the *Ns* H-NOX/BAY 58-2667 complex. Residues with CEST are colored with cyan. (For interpretation of the references to color in this figure legend, the reader is referred to the Web version of this article.)

following pretreatment of the cells with ODQ.

This pattern of heme-dependent (SNP) and heme-independent (BAY 60-2770) agonist sensitivity to ODQ was seen irrespective of the specific cell background, since similar results were obtained in the human prostate cancer cell line LnCaP (Suppl. data Fig. 6B) (Haramis et al., 2008).

As stated above, we eliminated by NMR methodology the possibility of direct chemical modification of either BAY 58-2667 or BAY 60-2770

by L-ascorbate (results not shown). By itself, ascorbate did not significantly modulate basal cGMP levels.

L-ascorbate was added in ODQ-naïve or ODQ-pretreated A7r5 cells simultaneously with the sGC activator (BAY 58-2667 or BAY 60-2770) and cell cGMP content was determined 15 min later. ODQ predictably potentiated the effect of both activators (the individual experiments are shown in Suppl. data Fig. 7, from which the data shown in Fig. 7 are

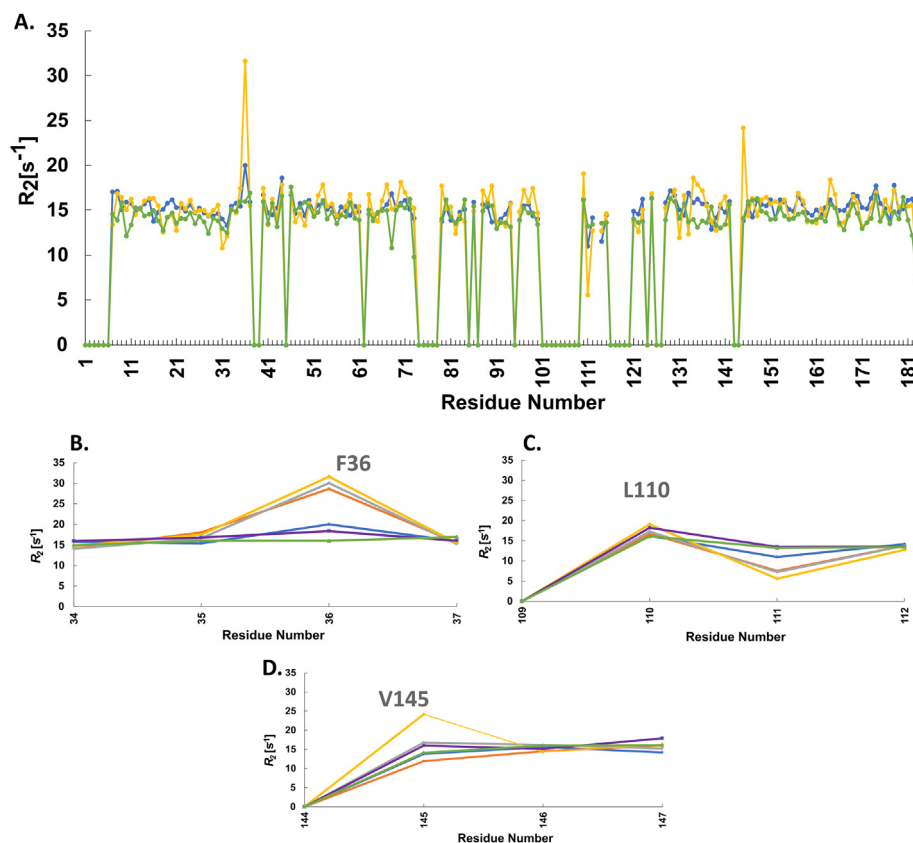


Fig. 5. A. R_2 rate constants of *Ns* H-NOX are shown for heme-bound state (blue), at protein/BAY 58-2667 ratio of 1:1 (yellow) and final BAY 58-2667 complex (green) B-D. Expanded regions for F36, L110, V145. protein/BAY 58-2667 ratio: 1:0.2 (orange), 1:0.5 (grey), 1:5 (purple). Residues with $R_2 = 0$ corresponds to unassigned residues of heme-bound *Ns* H-NOX. (For interpretation of the references to color in this figure legend, the reader is referred to the Web version of this article.)

derived). As seen in Fig. 7A, when the increases of cGMP are taken each time (i.e. with or out ODQ) as 1.0, the simultaneous addition of L-ascorbate with BAY 58-2667 does not significantly modulate the ability of the agonist to activate the sGC, in either oxidative or not conditions.

Ascorbate did not modulate the cGMP-raising effect of BAY 60-2770 in the absence of ODQ, either. However, in contrast to what was seen with BAY 58-2667, in ODQ-pretreated A7r5 cells L-ascorbate significantly reduced the response to BAY 60-2770 by $24 \pm 9\%$ (Fig. 7B). Again, the individual experiments summarized in Fig. 7 are given in Suppl. data Fig. 7.

These results are in agreement with our NMR data (Fig. 6) and suggest that the previously oxidized heme can, when its oxidation is opposed, to be re-inserted in the H-NOX cavity and thus dampen the ability of a potent sGC activator (BAY 60-2770) to occupy the same space and stimulate the enzyme. The re-introduction of reduced heme *per se* did not result in higher sGC enzymatic activity, since no heme-dependent agonist, such as an NO donor (e.g. SNP) or a stimulator molecule (e.g. BAY 41-2272) was present. It is noteworthy that in terms of sensitivity to L-ascorbate, the two activators are not equivalent in our biological system, despite their chemical/structural similarity and the NMR analysis-based ability to form relatively rigid complexes with H-NOX. It also stands to reason that the effect of the L-ascorbate cannot be attributed to a spurious, non-selective action on targets influencing indirectly cGMP levels, since a) it did not modulate the cGMP level induction by BAY 60-2770 in the absence of ODQ, and b) it affected only BAY 60-2770 responses but not those elicited by the related agonist BAY 58-2667.

To investigate this effect of L-ascorbate on BAY 60-2770 further, we focused only on cells pretreated with ODQ (i.e. following heme oxidation), by varying the time-point of ascorbate addition relatively to BAY 60-2770. To be able to do this, we prolonged from 15 min to 45 min the time allowed to BAY 60-2770 to stimulate the sGC and added L-ascorbate

either simultaneously with the activator as before (time 0) or 10 min and 20 min *after* the addition of BAY 60-2770 to the cells. The simultaneous addition of L-ascorbate significantly reduced, again, the sGC activator's effect, this time by $40 \pm 11\%$ (Fig. 8). When L-ascorbate was added 10 min after BAY 60-2770 this reduction was smaller, but still significant ($15 \pm 8\%$). Finally, addition of L-ascorbate 20min after the activator failed to diminish the agonist's effect, indicating a highly time-sensitive mode of interference (Fig. 8). Of note, when L-ascorbate was introduced 15min *before* BAY 60-2770, the reduction of the sGC activator's effect was $\sim 25\%$, which is similar to the reduction seen when added simultaneously with BAY 60-2770 (K. Salagiannis and S. Topouzis, results not shown).

The most straightforward interpretation of our data is that the closer L-ascorbate is present temporally to the addition of BAY 60-2770, the better it can enhance the ability of reduced heme to re-insert itself in the sGC H-NOX cavity and thus prevent, by steric hindrance, the insertion of the sGC activator, since the occupancy of this space by the heme moiety and the activator are thought to be mutually exclusive. Together with the structural data we provide (Fig. 6), they suggest that a highly dynamic, bi-directional (i.e. reversible) BAY 60/H-NOX interaction can take place and that the reduced heme and BAY 60-2770 are in constant antagonism for occupation of the protein regulatory cavity.

The different sensitivity of BAY 58-2667 and BAY 60-2770 to the effect of L-ascorbate raises questions pertinent to their respective use *in vivo*, where the redox status of the heme moiety is in constant flux, in response to the (patho)physiological cellular environment.

4. Discussion

The study of the dynamics and the conformational properties of the *Ns* H-NOX domain in different bound states allows us to identify the conformational exchange of H-NOX regions in different time scales as

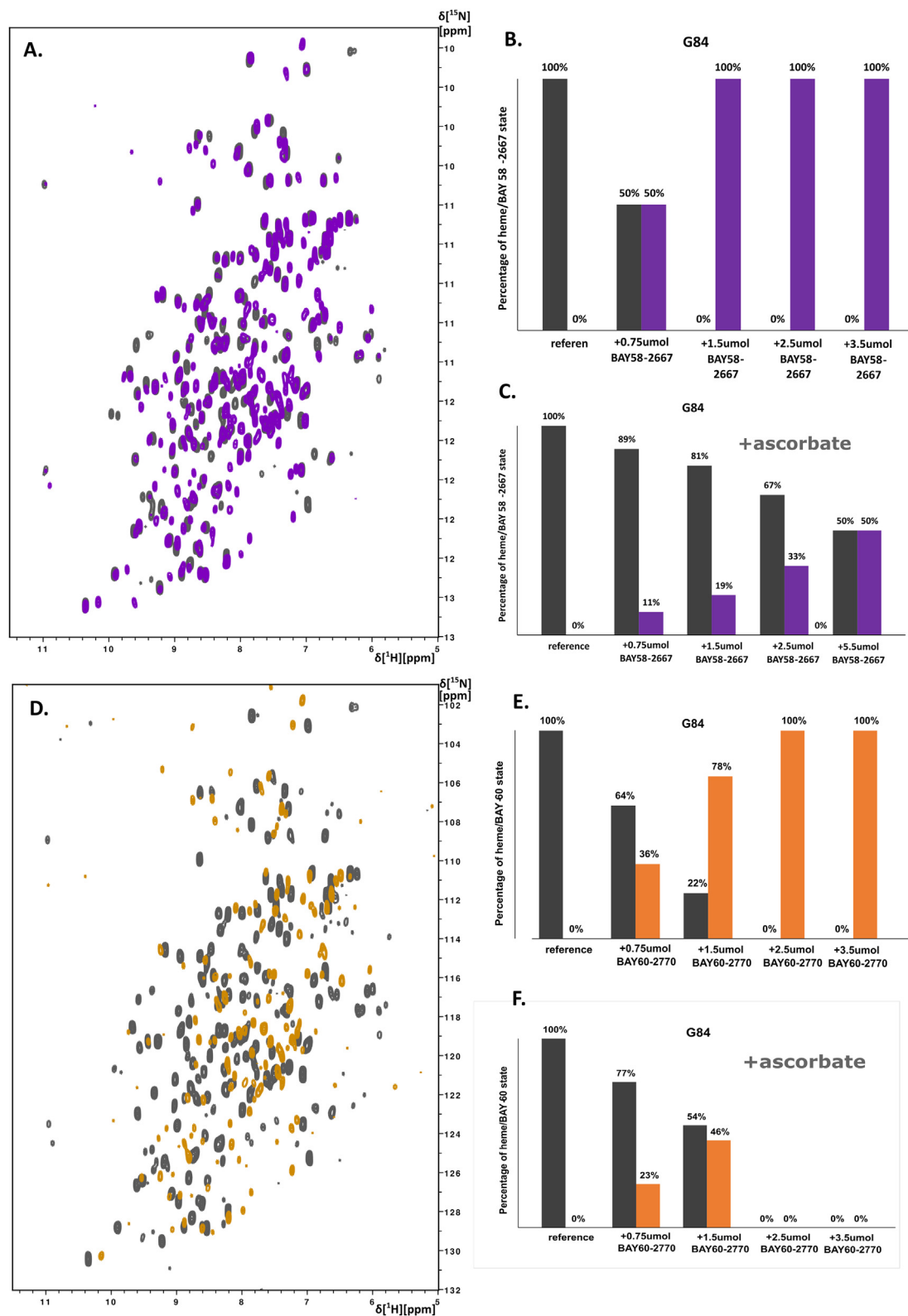


Fig. 6. A) Overlay of 1H - ^{15}N HSQC spectra of the *Ns* H-NOX domain in heme-bound state (grey) and BAY 58-2667 with 5 mM L-ascorbate (L-Asc) (purple). B) Percentage of heme (grey) and BAY 58-2667 (purple) bound states of *Ns* H-NOX during the titration experiment and C) in the presence of 5 mM L-Asc. D) Overlay of 1H - ^{15}N HSQC spectra of the *Ns* H-NOX domain in heme-bound state (grey) and BAY 60-2770 with 5 mM L-Asc (orange). E) Percentage of heme (grey) and BAY 60-2770 (orange) bound states of *Ns* H-NOX during the titration experiment and F) in the presence of 5 mM L-Asc. (For interpretation of the references to color in this figure legend, the reader is referred to the Web version of this article.)

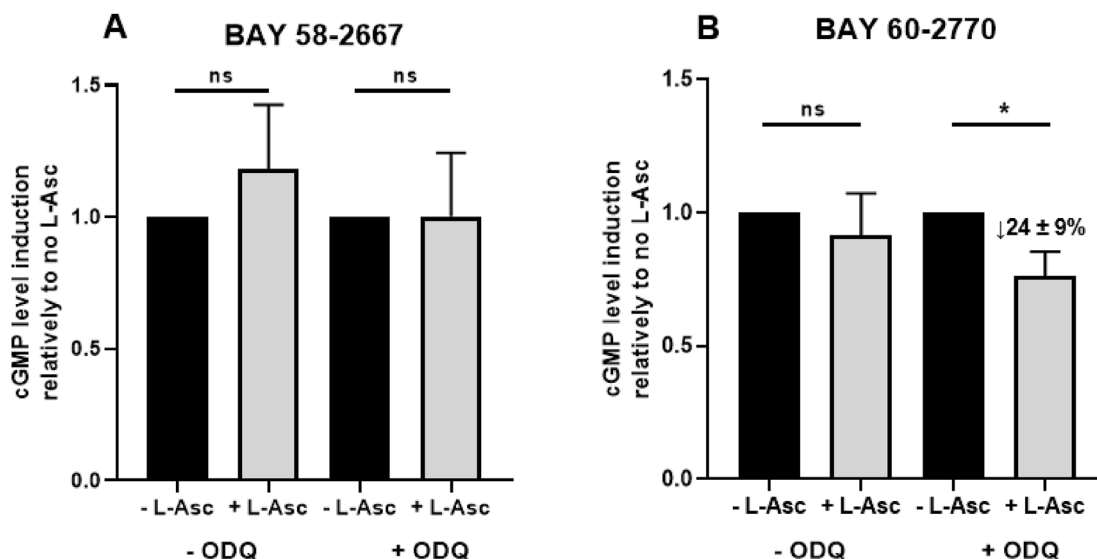


Fig. 7. Effect of simultaneous addition of L-Asc on the sGC activation by (A) BAY 58-2667 and (B) BAY 60-2770 in A7r5 cells. Cells were pretreated or not with the heme-oxidant ODQ (10 μ M). The sGC activators BAY 58-2667 and BAY 60-2770 (10 μ M) were added either alone or together with 1 mM L-Asc. 15 min later, cell extracts were taken, analyzed for cGMP content and normalized for total protein. Data are expressed as means \pm standard deviations of n=6 determinations, in 3 independent experiments. P values were determined by 2-tailed Student's t-test. A) The effect of BAY 58-2667 in the absence of L-Asc was taken each time as 1.0, either in the absence or in the presence of ODQ. B) The effect of BAY 60-2770 in the absence of L-Asc was taken each time as 1.0, either in the absence or in the presence of ODQ. *: p<0.05 relative to BAY 60-2770 treatment in the absence of L-Asc.

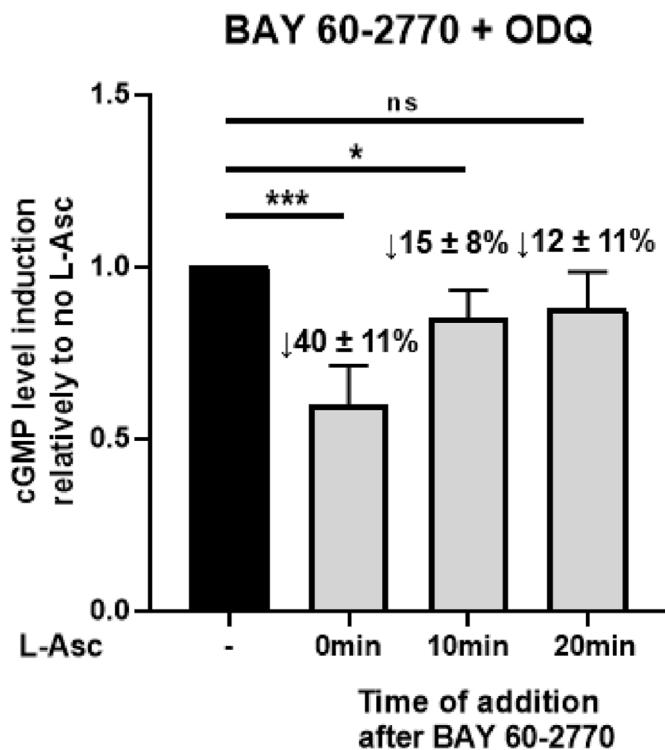


Fig. 8. Effect of delayed addition of L-ascorbate (L-Asc) on the sGC activation by BAY 60-2770 in A7r5 cells. Cells were pretreated with the heme-oxidant ODQ (10 μ M). The sGC activator BAY 60-2770 (10 μ M) was added while L-Asc (1 mM) was added either simultaneously (0 min) or 10 and 20 min after the activator. 45 min after the addition of BAY 60-2770, cell extracts were taken, analyzed for cGMP content and normalized for total protein. Data are expressed as means \pm standard deviations of n= 6 determinations obtained in 3 independent experiments. cGMP increases by BAY 60-2770 in the absence of L-Asc were taken as 1.0. P values were determined by 2-tail Student's t-test. *: p<0.05,***: p<0.001 relative to BAY 60-2770 treatment in the absence of L-Asc.

they are happening, providing insights at how this exchange could impact the resulting biological processes. The striking correspondence between the ps-ns dynamics and the CEST experiment corroborates our hypothesis that the heme is responsible for the great dynamic behavior of the protein, while its replacement by the synthetic sGC activators seems to invert this condition and lead the protein to a more compact state. It is known that the activation of sGC enzyme is triggered by the binding of either NO or other agonists, including sGC “activators”. Since the heme-independent activation of the sGC enzyme by “activators” necessitates a concomitant replacement of the heme, it is very intriguing that the native H-NOX and the BAY - H-NOX 3D structures are pretty similar (rmsd *Ns* H-NOX-heme/BAY 58-2667: 0.37 and *Ns* H-NOX-heme/BAY 60-2770: 0.33). Therefore, we hypothesize that structural dynamics play a significant role in the activation of the enzyme, while the transition from a highly dynamic, heme-bound state to a more rigid protein state provides novel insights in this, still poorly explored, biological process. In the absence of the any atomic-level information about the dynamics of the sGC H-NOX region, either in its native, heme-loaded state, or in complex with BAYs, we provide convincing experimental evidence that heme replacement by the activators, the H-NOX domain loses a significant part of its conformational plasticity. Indeed, as reported above, the dynamics at ps-ns time scales are typical of a compact and rigid structure. The fact that there is no observable second conformational state in the H-NOX - BAY 58-2667 complex, combined with the observation that only a few H-NOX residues are found to undergo a conformational exchange process, suggest that in the presence of BAY 58-2667 the H-NOX protein exhibits an even less dynamic structure in a wide range of time-scales. All the above, along with the similar conformational features of all available crystal structures, indicate that additional processes or changes, that are not observable either by X-ray or by NMR dynamics methodology, may be crucially involved in the activated, but conformationally rigid, H-NOX domain in complex with the BAY activators.

This may be attributed to the complete exchange event between the heme and the BAY 58-2667 during the formation of the final complex with the compound. According to our NMR data, this heme-BAY exchange process is faster than the NMR time-scale allows to observe and NMR methodology can only observe the presence of the new, stable, BAY - H-NOX complex, formed immediately after the activator's addition in

the heme-H-NOX solution. Combination of different approaches identified the “hot spots”, such as D35-F37, E41-T48, L110-L115 and V145-G147, of the *Ns* H-NOX domain in complex with two different ligands and revealed dynamics in several time scales. These protein regions adopt low-populated conformational states and may facilitate the initiation of the heme-sGC activator exchange process. This study, in combination with further NMR relaxation experiments of mutants or with other ligands, aided by functional approaches, can provide unprecedented insight into the mechanism of activation of the sGC enzyme and the structural constraints regulating the NO/sGC/cGMP signaling pathway. This need for understanding may not be adequately addressed by the conformational features and the overall 3D fold of the H-NOX domain provided by structure determination via X-ray crystallography or conventional NMR methods. The dynamic properties of the H-NOX protein domain reveals differences regarding the modes of sGC activation by NO and by sGC activators, thus deciphering the enzyme's function and enabling the design of novel, “tailored” agonist compounds.

Arguably, the most important proximal regulator (or “gate-keeper”) of the activator molecules' bioactivity is the redox state of the heme moiety (reviewed in Follmann et al., 2013). The current work reveals that the association of an activator compound (heme- and NO-independent) with the sGC enzyme can be modulated reversibly by heme's redox status. In recent years, it has been shown that the sGC dimer enzyme does not exist in cells and tissues all in a heme-associated or a heme-devoid form, but these two functionally distinct forms coexist and their presence constantly reflects the cellular environment (Stuehr et al., 2021; Sandner et al., 2021, Ghosh & Stuehr, 2017).

The predominant current view on the activity of potent sGC activators, such as the two BAYER molecules, is that their association with sGC is “stable” (Sömmer et al., 2018) or essentially “irreversible” (Kollau et al., 2018). Therefore, the fact that L-ascorbate can indirectly affect this association, presumably by promoting the reversal of heme's oxidation, was unexpected. This was seen in both the structural studies, where the rigidity of the BAY/H-NOX complex collapses upon addition of L-ascorbate (Fig. 6), as well as in the cell-based studies, by the time-sensitive reduction of BAY 60's activity (Figs. 7B and 8, Suppl. data Fig. 7). Together, these data point to an up-to-now largely unsuspected reversibility of the sGC agonist/H-NOX association, since the bound activator can be displaced by ferrous heme. Overall, therefore, the interaction is a lot more dynamic than previously thought, regulated by bi-directional competition between reduced heme and BAY molecules for the H-NOX cavity making.

Based on the divergent behavior of the two structurally related sGC activators shown here, we propose that any future successful design of novel activator molecules should be based on an extensive characterization of the fluctuating tissue content of heme-loaded and heme-devoid sGC forms in the targeted disease and take into serious consideration the variable experimental sensitivity of the compounds to the redox status of the heme, which is in osmosis with the cellular environment.

Funding sources

We acknowledge support of this work by the project “INSPIRED-The National Research Infrastructures on Integrated Structural Biology, Drug Screening Efforts and Drug target functional characterization” (MIS 5002550) which is implemented under the Action “Reinforcement of the Research and Innovation Infrastructure”, funded by the Operational Programme “Competitiveness, Entrepreneurship and Innovation” (NSRF, 2014-2020) and co-financed by Greece and the European Union (European Regional Development Fund). Georgios Dalkas acknowledges Marie Skłodowska-Curie Individual Grant (“NMRSIGN”-795175). EU FP7 REGPOT CT-2011-285950 – “SEE-DRUG” project is acknowledged for the purchase of UPAT's 700 MHz NMR equipment.

CRediT authorship contribution statement

Aikaterini I. Argyriou: Methodology, Investigation, Resources, writing. **Garyfallia I. Makrynitsa:** Methodology, Investigation, Resources, writing. **Georgios Dalkas:** Methodology, Investigation, writing. **Dimitra A. Georgopoulou:** Methodology, Investigation, Resources. **Konstantinos Salagiannis:** Methodology, Investigation, Resources, writing. **Vassiliki Vazoura:** Methodology, Investigation, Resources, writing. **Andreas Papapetropoulos:** Conceptualization, writing. **Stavros Topouzis:** Conceptualization, Investigation, writing. **Georgios A. Spyroulias:** Conceptualization, Supervision, Funding acquisition, Investigation, writing.

Declaration of competing interest

The authors declare the following financial interests/personal relationships which may be considered as potential competing interests: Georgios A. Spyroulias reports financial support was provided by European Community. Georgios Dalkas reports financial support was provided by European Community. Georgios A. Spyroulias reports was provided by Greek General Secretariat of Research & Technology.

Acknowledgements

We are indebted to Dr. Peter Sandner (BAYER AG, Wuppertal, Germany) for the generous gift of BAY 58-2667 and BAY 60-2770.

Appendix A. Supplementary data

Supplementary data to this article can be found online at <https://doi.org/10.1016/j.crstbi.2021.11.003>.

References

- Alderson, T.R., Kay, L.E., 2020. Unveiling invisible protein states with NMR spectroscopy. *Curr. Opin. Struct. Biol.* 60, 39–49.
- Alexandropoulos, I.I., Argyriou, A.I., Marousis, K.D., Topouzis, S., Papapetropoulos, A., Spyroulias, G.A., 2016. 1 H, 13 C, 15 N backbone and side-chain resonance assignment of Nostoc sp. C139A variant of the heme-nitric oxide/oxygen binding (H-NOX) domain. *Biomol. NMR Assign.* 10 (2), 395–400.
- Breitenstein, S., Roessig, L., Sandner, P., Lewis, K.S., 2016. Novel sGC stimulators and sGC activators for the treatment of heart failure. *Handb. Exp. Pharmacol.* 243, 225–247.
- Case, D., et al., 2018. (The amber project, 2018). Amber.
- Chester, M., Seedorf, G., Tourmeux, P., Gien, J., Tseng, N., Grover, T., Wright, J., Stasch, J.P., Abman, S.H., 2011. Cinaciguat, a soluble guanylate cyclase activator, augments cGMP after oxidative stress and causes pulmonary vasodilation in neonatal pulmonary hypertension. *Am. J. Physiol. Lung Cell Mol. Physiol.* 301 (5), 755–764.
- Dang, T.A., Schunkert, H., Kessler, T., 2020. cGMP signaling in cardiovascular diseases: linking genotype and phenotype. *J. Cardiovasc. Pharmacol.* 75 (6), 516–525.
- Darden, T., York, D., Pedersen, L., 1993. Particle mesh Ewald: an N-log(N) method for Ewald sums in large systems. *J. Chem. Phys.* 98 (12), 10089.
- Dasgupta, A., Bowman, L., D'Arsigny, C.L., Archer, S.L., 2015. Soluble guanylate cyclase: a new therapeutic target for pulmonary arterial hypertension and chronic thromboembolic pulmonary hypertension. *Clin. Pharmacol. Ther.* 97 (1), 88–102.
- Eisenmesser, E.Z., Bosco, D.A., Akke, M., Kern, D., 2002. Enzyme dynamics during catalysis. *Science* 295 (5559), 1520–1523.
- Evgenov, O.V., Pacher, P., Schmidt, P.M., Haskó, G., Schmidt, H.H.H.W., Stasch, J.P., 2006. NO-independent stimulators and activators of soluble guanylate cyclase: discovery and therapeutic potential. *Nat. Rev. Drug Discov.* 5 (9), 755–768.
- Follmann, M., Griebenow, N., Hahn, M.G., Hartung, I., Mais, F.J., Mittendorf, J., Schäfer, M., Schiroke, H., Stasch, J.P., Stoll, F., Straub, A., 2013. The chemistry and biology of soluble guanylate cyclase stimulators and activators. *Angew Chem. Int. Ed. Engl.* 52 (36), 9442–9462.
- Gheorghiadu, M., Marti, C.N., Sabbah, H.N., Roessig, L., Greene, S.J., Böhm, M., Collins, S.P., 2013. Soluble guanylate cyclase: a potential therapeutic target for heart failure. *Heart Fail. Rev.* 18 (2), 123–134.
- Ghofrani, H.-A., D'Armini, A.M., Grimminger, F., Hoepfer, M.M., Jansa, P., Kim, N.H., Wang, C., 2013. Riociguat for the treatment of chronic thromboembolic pulmonary hypertension. *N. Engl. J. Med.* 369 (4), 319–329.
- Ghosh, A., Stasch, P.J., Papapetropoulos, A., Stuehr, D.J., 2014. Nitric oxide and heat shock protein 90 activate soluble guanylate cyclase by driving rapid change in its subunit interactions and heme content. *J. Biol. Chem.* 289 (22), 15259–15271.
- Ghosh, A., Stuehr, D.J., 2017. Regulation of sGC via hsp90, cellular heme, sGC agonists, and NO: new pathways and clinical perspectives. *Antioxidants Redox Signal.* 26 (4), 82–190.

- Haramis, G., Zhou, Z., Pyriochou, A., Koutsilieris, M., Roussos, C., Papapetropoulos, A., 2008. cGMP-independent anti-tumour actions of the inhibitor of soluble guanylyl cyclase, ODQ, in prostate cancer cell lines. *Br. J. Pharmacol.* 155 (6), 804–813.
- Hoffmann, L.S., Schmidt, P.M., Keim, Y., Schaefer, S., Schmidt, H.H.H.W., Stasch, J.P., 2009. Distinct molecular requirements for activation or stabilization of soluble guanylyl cyclase upon haem oxidation-induced degradation. *Br. J. Pharmacol.* 157 (5), 781–795.
- Holt, A.W., Martin, D.N., Shaver, P.R., Adderley, S.P., Stone, J.D., Joshi, C.N., Francisco, J.T., Lust, R.M., Weidner, D.A., Shewchuk, B.M., Tulis, D.A., 2016. Soluble guanylyl cyclase-activated cyclic GMP dependent protein kinase inhibits arterial smooth muscle cell migration independent of VASP-serine 239 phosphorylation. *Cell. Signal.* 28 (9), 1364–1379.
- Humphrey, W., Dalke, A., Schulten, K., 1996. VMD: visual molecular dynamics. *J. Mol. Graph.* 14 (1), 33–38.
- Jakalian, A., Jack, D.B., Bayly, C.I., 2002. Fast, efficient generation of high-quality atomic charges. AM1-BCC model: II. Parameterization and validation. *J. Comput. Chem.* 23 (16), 1623–1641.
- Keller, R., 2004. The Computer Aided Resonance Assignment Tutorial. ISBN 3-85600-112-3, 30, p. 2011. Accessed September.
- Kollau, A., Opelt, M., Wölkart, G., Gorren, A.C.F., Russwurm, M., Koesling, D., Mayer, B., Schrammel, A., 2018. Irreversible activation and stabilization of soluble guanylate cyclase by the protoporphyrin IX mimetic cinaciguat. *Mol. Pharmacol.* 93 (2), 73–78.
- Kumar, V., Martin, F., Hahn, M.G., Schaefer, M., Stämmer, J.S., Stasch, J.-P., van den Akker, F., 2013. Insights into BAY 60-2770 activation and S-nitrosylation-dependent desensitization of soluble guanylyl cyclase via crystal structures of homologous nostoc H-NOX domain complexes. *Biochemistry* 52 (20), 3601–3608.
- Li, P., Merz, K.M., 2016. MCPB.py: a Python based metal center parameter builder. *J. Chem. Inf. Model.* 56 (4), 599–604.
- Liu, R., Kang, Y., Chen, L., 2021. Activation mechanism of human soluble guanylate cyclase by stimulators and activators. *Nat. Commun.* 12 (1).
- Ma, X., Sayed, N., Beuve, A., Van Den Akker, F., 2007. NO and CO differentially activate soluble guanylyl cyclase via a heme pivot-bend mechanism. *EMBO J.* 26 (2), 578–588.
- Maier, J.A., Martinez, C., Kasavajhala, K., Wickstrom, L., Hauser, K.E., Simmerling, C., 2015. ff14SB: improving the accuracy of protein side chain and backbone parameters from ff99SB. *J. Chem. Theor. Comput.* 11 (8), 3696–3713.
- Makrynitsa, G.I., Argyriou, A.I., Dalkas, G., Georgopoulou, D.A., Bantzi, M., Giannis, A., Papapetropoulos, A., Spyroulias, G.A., 2021. Backbone and side chain NMR assignments of the H-NOX domain from Nostoc sp. in complex with BAY58-2667 (cinaciguat). *Biomol. NMR Assign.* 15 (1), 53–57.
- Makrynitsa, G.I., Zompra, A.A., Argyriou, A.I., Spyroulias, G.A., Topouzis, S., 2019. Therapeutic targeting of the soluble guanylate cyclase. *Curr. Med. Chem.* 26 (15), 2730–2747.
- Martin, F., Baskaran, P., Ma, X., Dunten, P.W., Schaefer, M., Stasch, J.-P., Beuve, A., Van Den Akker, F., 2010. Structure of cinaciguat (BAY 58–2667) bound to Nostoc H-NOX domain reveals insights into heme-mimetic activation of the soluble guanylyl cyclase. *J. Biol. Chem.* 285 (29), 22651–22657.
- Mittendorf, J., Weigand, S., Alonso-Alija, C., Bischoff, E., Feurer, A., Gerisch, M., Muentzer, K., 2009. Discovery of riciquat (BAY 63-2521): a potent, oral stimulator of soluble guanylate cyclase for the treatment of pulmonary hypertension. *ChemMedChem* 4 (5), 853–865.
- Papapetropoulos, A., Hobbs, A.J., Topouzis, S., 2015. Extending the translational potential of targeting NO/cGMP-regulated pathways in the CVS. *Br. J. Pharmacol.* 172 (6), 1397–1414.
- Pettersen, E.F., Goddard, T.D., Huang, C.C., Couch, G.S., Greenblatt, D.M., Meng, E.C., Ferrin, T.E., 2004. UCSF Chimera—a visualization system for exploratory research and analysis. *J. Comput. Chem.* 25 (13), 1605–1612.
- Prompers, J.J., Brüschweiler, R., 2002. General framework for studying the dynamics of folded and non folded proteins by NMR relaxation spectroscopy and MD simulation. *J. Am. Chem. Soc.* 124 (16), 4522–4534.
- Roe, D.R., Cheatham, T.E., 2013. PTRAJ and CPPTRAJ: software for processing and analysis of molecular dynamics trajectory data. *J. Chem. Theor. Comput.* 9 (7), 3084–3095.
- Ryckaert, J.P., Ciccotti, G., Berendsen, H.J.C., 1977. Numerical integration of the cartesian equations of motion of a system with constraints: molecular dynamics of n-alkanes. *J. Comput. Phys.* 23, 327–341.
- Sandner, P., Zimmer, D.P., Milne, G.T., Follmann, M., Hobbs, A., Stasch, J.P., 2021. Soluble guanylate cyclase stimulators and activators. *Hand. Exp. Pharmacol.* 264, 355–394.
- Schindler, U., Strobel, H., Schönafinger, K., Linz, W., Löhn, M., Martorana, P.A., Sohn, M., 2006. Biochemistry and pharmacology of novel anthranilic acid derivatives activating heme-oxidized soluble guanylyl cyclase. *Mol. Pharmacol.* 69 (4), 1260–1268.
- Sömmer, A., Sandner, P., Behrends, S., 2018. BAY 60–2770 activates two isoforms of nitric oxide sensitive guanylyl cyclase: evidence for stable insertion of activator drug. *Biochem. Pharmacol.* 147, 10–20.
- Stasch, J.-P., Schmidt, P.M., Nedvetskaya, T.Y., Hs, A.K., Meurer, S., Lapp, H., 2006. Targeting the heme-oxidized nitric oxide receptor for selective vasodilatation of diseased blood vessels. *J. Clin. Invest.* 116 (9), 2552–2561.
- Stuehr, D.J., Misra, S., Dai, Y., Ghosh, A., 2021. Maturation, inactivation, and recovery mechanisms of soluble guanylyl cyclase. *J. Biol. Chem.* 296, 100336.
- da Silva, A.W.S., Vranken, W.F., 2012. ACPYPE - AnteChamber PYthon parser interface. *BMC Res. Notes* 5, 367.
- Vallurupalli, P., Bouvignies, G., Kay, L.E., 2012. Studying “invisible” excited protein states in slow exchange with a major state conformation. *J. Am. Chem. Soc.* 134 (19), 8148–8161.
- Wang, J., Wolf, R.M., Caldwell, J.W., Kollman, P.A., Case, D.A., 2004. Development and testing of a general amber force field. *J. Comput. Chem.* 25 (9), 1157–1174.
- Williamson, M.P., 2013. Using chemical shift perturbation to characterise ligand binding. *Prog. Nucl. Magn. Reson. Spectrosc.* 73, 1–16.
- Wittenborn, E.C., Marletta, M.A., 2021. Structural perspectives on the mechanism of soluble guanylate cyclase activation. *Int. J. Mol. Sci.* 22 (11), 5439.
- Zhou, Z., Pyriochou, A., Kotanidou, A., Dalkas, G., van Eickels, M., Spyroulias, G.A., Roussos, C., Papapetropoulos, A., 2008. Soluble guanylyl cyclase activation by HMR-1766 (ataciguat) in cells exposed to oxidative stress. *Am. J. Physiol. Heart Circ. Physiol.* 295 (4), 1763–1771.